


## COMMUNICATION

Cite this: *Nanoscale Adv.*, 2020, 2, 4417Received 24th April 2020  
Accepted 18th August 2020

DOI: 10.1039/d0na00327a

rsc.li/nanoscale-advances

**Bottom-up synthesis of nitrogen-doped nanocarbons by a combination of metal catalysis and a solution plasma process†**Yang Zhou<sup>a</sup> and Yuta Nishina<sup>ab</sup> 

We aimed to develop the bottom-up synthesis of nanocarbons with specific functions from molecules without any leaving group, halogen atom and boronic acid, by employing a metal catalyst under solution plasma irradiation. Pyridine was used as a source of carbon. In the presence of a Pd catalyst, the plasma treatment enabled the synthesis of N-doped carbons with a pyridinic configuration, which worked as an active catalytic site for the oxygen reduction reaction.

Carbon has great potential to replace metal-based products, such as catalysts,<sup>1</sup> supercapacitors,<sup>2</sup> and lithium-ion batteries,<sup>3</sup> because of the defined structure and surface properties. It is expected to be a next-generation material.<sup>4</sup> In particular, nanocarbons have been extensively studied due to their outstanding physical and chemical properties that are different from those of bulk carbons.<sup>5</sup> Nanocarbon synthesis methods are roughly classified into two types: top-down and bottom-up methods (Table S1†).<sup>6–9</sup> Examples of the former method are solid-state ball milling<sup>10</sup> and liquid-phase exfoliation (LPE) of bulk carbons,<sup>11,12</sup> such as coal and graphite. The top-down method is mass producible and straightforward; however, the control of the fine structure is an issue to be solved. The bottom-up methods<sup>13</sup> are further classified into three types: organic synthesis,<sup>14</sup> chemical vapor deposition (CVD),<sup>15</sup> and solution plasma (SP) treatment.<sup>16</sup> Organic synthesis has recently attracted much attention due to the precise controllability of nanocarbon structures.<sup>17</sup> However, it requires multiple steps and specially designed starting molecules bearing reactive functional groups, such as halogens and boronic acids, rendering difficulty in mass production and practical application. CVD methods are generally used to form carbon nanotubes and graphene in the presence of a metal

catalyst or metal substrate. Due to the high temperature under controlled pressure, highly crystalline nanocarbons can be formed by CVD, whereas starting molecules are decomposed to the elemental level during the process, abandoning most of the original molecular structure. The SP process is an emerging method of nanocarbon synthesis in which a solution of organic molecules is subjected to a pulsed glow discharge. Due to the high energy of plasma, aromatic compounds without any leaving group can be used as a source of carbon. However, the SP method also mostly abandons the original structure of starting molecules (Table S1†). To fulfill the requirements for structure controllability and mass production in nanocarbon synthesis, we investigated combinations of various methods. As a result, we found that employing a metal catalyst under SP irradiation enabled the production of nanocarbons from a simple molecule without any leaving group while keeping its original structure. In this manuscript, we term this method the metal-catalyzed solution plasma (MCSP) method.

Until now, there has been no report on the preparation of nanocarbons using the MCSP method. Fig. 1a shows a picture of the SP generation system. A tungsten electrode (Nilaco Co, Japan, Ø1.0 mm 99.95%) wrapped with an insulating ceramic tube (Nilaco Co, Japan, Ø2.0 × 1.0 mm) was inserted on both sides of a glass container with an electrode distance of 1 mm. The starting molecule, solvent, and catalyst were added to the reactor, and a bipolar pulse power supply was connected to generate an SP with a pulse width of 1 µs and a pulse frequency of 26 kHz. The discharge was continued while stirring. Then, the nanocarbon products were collected by filtration followed by washing with organic solvents, and water three times respectively to remove soluble compounds. Finally, the nanocarbon product was collected.

Fig. 1b–e show the formation of carbon as the reaction proceeded. Since SP treatment is a high-energy process, molecules cannot be carbonized with maintaining their original structure. Therefore, controlling the SP irradiation conditions should be carefully optimized. During the SP treatment, aromatic hydrocarbons are readily carbonized, but aliphatic hydrocarbons are

<sup>a</sup>Graduate School of Natural Science and Technology, Okayama University, 3-1-1, Tsushima-naka, Kita-ku, Okayama, 700-8530, Japan. E-mail: nisina-y@cc.okayama-u.ac.jp

<sup>b</sup>Research Core for Interdisciplinary Sciences, Okayama University, 3-1-1, Tsushima-naka, Kita-ku, Okayama, 700-8530, Japan

† Electronic supplementary information (ESI) available. See DOI: 10.1039/d0na00327a



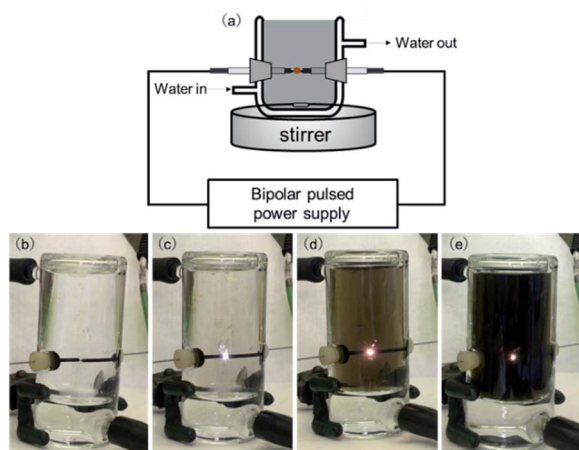
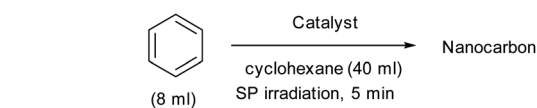


Fig. 1 (a) Experimental setup of SP irradiation, and (b–e) Photos of the experiment performed.

Table 1 Effect of the catalyst on carbonization of benzene in cyclohexane by SP irradiation<sup>a</sup>



Entry	Catalyst	Product <sup>b</sup> (mg)
1	None	119.6
2	Pd(OAc) <sub>2</sub> (0.5 mmol)	140.3
3	Fe(OAc) <sub>3</sub> ·nH <sub>2</sub> O (0.5 mmol)	111.4
4	FeCp <sub>2</sub> (0.5 mmol)	110.5
5	Cu(OAc) <sub>2</sub> ·H <sub>2</sub> O (0.5 mmol)	112.3

<sup>a</sup> The mixture of benzene (8 ml) and cyclohexane (40 ml) was irradiated by SP for 5 min in the presence of a metal catalyst under water cooling.

<sup>b</sup> After discharging for 5 min with stirring, the obtained solution was transferred into a flask to remove the solvent by rotary evaporation. After being dried *in vacuo* at 60 °C for 15 h, the product mass was weighed.

less reactive under the SP conditions.<sup>18</sup> Consequently, we irradiated SP in cyclohexane using benzene as a model starting material. In the absence of any catalyst, 119.6 mg of carbon was obtained in 5 min (Table 1, entry 1). In the presence of a Pd catalyst, 140.3 mg of carbon was obtained, suggesting the high efficiency of the MCSP process (Table 1, entry 2). Other metal catalysts, such as Fe and Cu, did not contribute to increasing the carbon production (Table 1, entries 3–5). Although we tested only four different types of catalysts, we focused on the palladium acetate (Pd(OAc)<sub>2</sub>) catalyst in the following investigations, as it had the highest efficiency among them.

The mechanism of the carbonization is still unclear, but we hypothesize that the high-energy plasma conditions promote C–H bond activation of pyridine in the presence of Pd, and then Pd was oxidized by the plasma to a higher valence state. Finally, the reductive elimination of Pd generates the coupling product of pyridine. The catalytic cycles successively occur to promote the production of carbon frameworks.<sup>19,20</sup>

Table 2 Elemental analysis by XPS and Raman analyses of nanocarbons produced from with different amounts of the Pd catalyst

Nanocarbon	Elemental analysis by XPS <sup>a</sup>			Raman analysis
	C (at%)	O (at%)	N (at%)	I <sub>D</sub> /I <sub>G</sub>
C1	91.8	8.2	0	0.80
C2	79.0	20.5	0.5	0.93
C3	81.9	15.1	3.0	0.83
C4	82.1	13.9	4.0	0.94

<sup>a</sup> The mixture of pyridine (8 ml) and cyclohexane (40 ml) was irradiated by SP for 30 min in the presence of a metal catalyst under water cooling. The produced nanocarbon was filtered, washed with benzene, cyclohexane, acetone, and water, and then vacuum dried at 60 °C for 15 h before XPS and Raman analyses.

Next, to confirm the ability of the catalyst to maintain the original molecular skeleton, the characterization of the carbon products was performed. For this purpose, MCSP treatment was performed for pyridine. For comparison, SP treatment was performed without a catalyst. The elemental compositions of the generated carbons determined by X-ray photoelectron spectroscopy (XPS) are summarized in Table 2 and Fig. S1.† It was clarified that the nitrogen atom was not introduced into the carbon framework without a catalyst (C1), and it was assumed that the original molecular structure of pyridine was destroyed at the atomic level under the SP conditions (Fig. 2a). This result agrees with Saito's report.<sup>21</sup> On the other hand, nitrogen-containing carbons C2, C3, and C4 were obtained using 0.1 mmol, 0.3 mmol, and 0.5 mmol of Pd(OAc)<sub>2</sub> as a catalyst, respectively. As the amount of Pd increased, the nitrogen content in the carbon increased. More than 4% of nitrogen atoms were observed by using 0.5 mmol Pd(OAc)<sub>2</sub>, suggesting that the carbonization reaction proceeded without destroying the starting molecule with the aid of the catalyst (Fig. 2b).

Next, the crystallinity of the obtained carbons was evaluated by Raman spectroscopy analysis (Fig. 3a) and X-ray diffraction

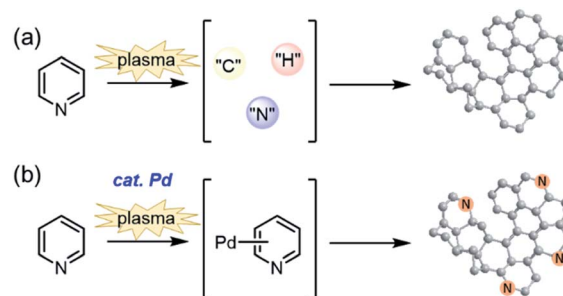


Fig. 2 Schematic illustrations of nanocarbon production by SP methods; (a) in the absence and (b) presence of the Pd catalyst.

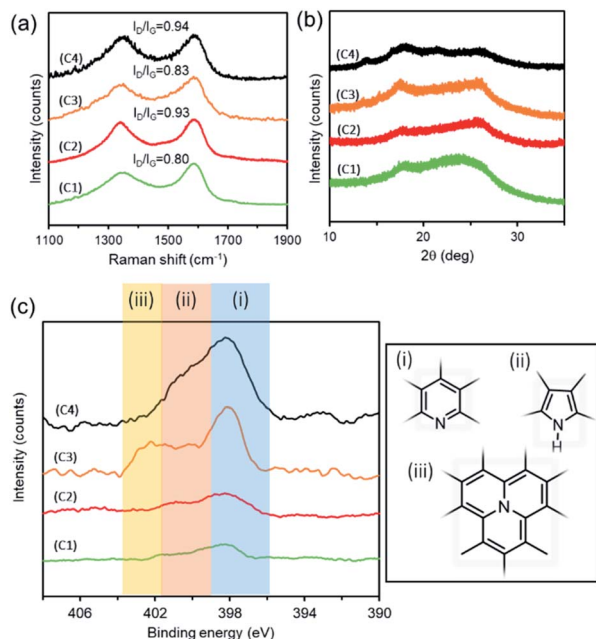


Fig. 3 (a) Raman spectra, (b) XRD patterns, and (c) XPS N 1s regions of C1–C4. (i): pyridinic; (ii): pyrrolic; (iii): graphitic nitrogen.

(XRD) analysis (Fig. 3b). In the Raman spectrum, two peaks corresponding to the G and D bands were observed at 1598–1600  $\text{cm}^{-1}$  and 1350–1353  $\text{cm}^{-1}$ , respectively. The G band is derived from the  $\text{sp}^2$  hybrid orbital (graphitic structure), and the D band is derived from structural disorder and defects. Therefore, a larger intensity ratio of the D band and G band ( $I_D/I_G$ ) means that more defects are present in the material and the crystallinity is low. The nanocarbons C1, C2, C3, and C4 showed  $I_D/I_G$  values of 0.80, 0.93, 0.83, and 0.94, respectively (Table 2, right column), suggesting the presence of many defects. In XRD, a broad signal was observed over  $2\theta = 15\text{--}30^\circ$ . From the above XRD and Raman measurements, it was found that all carbons C2, C3, and C4 were amorphous. XPS analysis in the N 1s region revealed that C4 prepared using the largest amount of  $\text{Pd}(\text{OAc})_2$  was mainly composed of pyridine-like nitrogen atoms (Fig. 3c and Table 3). This also supports the hypothesis that the MCSP

Table 3 XPS deconvolution analysis of nanocarbons<sup>a</sup>

Nanocarbon	The chemical state of nitrogen (at%)		
	Pyridinic (i)	Pyrrolic (ii)	Graphitic (iii)
C1	0	0	0
C2	21.6	43.8	34.6
C3	48.4	37.1	14.5
C4	62.5	22.3	15.2

<sup>a</sup> The mixture of pyridine (8 ml) and cyclohexane (40 ml) was irradiated by SP for 30 min in the presence of a metal catalyst under water cooling. The produced nanocarbon was filtered, washed with benzene, cyclohexane, acetone, and water, and then vacuum dried at 60 °C for 15 h before XPS and Raman analyses.

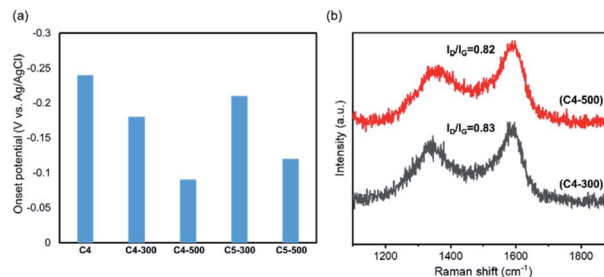


Fig. 4 (a) Onset potentials of the specimens. (b) Raman spectra of C4-300 and C4-500.

method promotes the carbonization while suppressing the destruction of the original structure of pyridine. We tried to confirm the presence of nitrogen functional groups by FT-IR, but satisfactory data were not obtained (Fig. S2†). The morphology of each carbon was analyzed by SEM and BET analysis (Fig. S3 and Table S2†). As a result, we confirmed the nano-sized carbon formation.

Nitrogen-doped carbons have potential applications as supercapacitors,<sup>22</sup> anode materials for sodium-ion batteries,<sup>23</sup> oxygen evolution reaction (OER) electrocatalysts,<sup>24</sup> and catalytic support materials.<sup>25</sup> In this research, we applied our nitrogen-containing nanocarbons as catalysts for the oxygen reduction reaction (ORR) (Fig. 4).<sup>26</sup> The nanocarbons produced from pyridine by MCSP, C1–C4, showed almost no ORR activity (Fig. S5†). Heat treatment significantly affected the catalytic performance. C4 was heated at 300 °C and 500 °C, and then increased ORR activity and output current density were observed (Fig. 4a). Although the performance was lower than that of the practical ORR catalyst (Pt/C), 500 °C-treated C4 showed an improved ORR potential of 0.09 V, which is superior to the  $-0.17$  V shown by the previously reported N-doped carbon.<sup>21</sup> XPS elemental analysis shows that the nitrogen content in C4 was reduced from 4.0% to 1.5% after the heat treatment at 500 °C (Fig. S6 and Table S3†). Raman spectra showed that the  $I_D/I_G$  values of C4-300 and C4-500 were 0.83 and 0.82, respectively (Fig. 4b). From these results it can be interpreted that the heat treatment did not cause much change to the crystallinity, and the increase in ORR activity might be attributed to the increase in the surface area (Table S2†) and electron conductivity.<sup>27</sup>

To elucidate the effect of doped nitrogen atoms, we compared the ORR performance between C4 and C5. C5 was synthesized using benzene as the raw material with the addition of the 0.5 mmol Pd catalyst. Then, the specimen was heated at 300 °C and 500 °C (C5-300 and C5-500). Their onset potentials were less than those of C4-300 and C4-500, respectively. Therefore, the doped pyridinic nitrogen atoms caused the difference of the potentials between C4-300 and C5-300. C4 also shows good activity for C–H activation (Table S4†), which is considered to be provided by a large number of free radicals in C4 (Fig. S7†).

## Conclusions

We developed the MCSP method as a new type of bottom-up nanocarbon production method. We confirmed that the carbon yield increased when Pd was used as the catalyst, and the nitrogen content was more than 4% when 0.5 mmol of the Pd catalyst was added. The nitrogen-containing carbon was applied as a catalyst for the ORR, and improved catalytic activity was obtained after heat treatment. Since these applications led to the replacement of conventional metallic materials and the reduction of their use, this method can contribute to solving the resource depletion problem, which is a concern for the future. The formation mechanism of nanocarbons under MCSP treatment will be investigated in detail in our next study.

## Conflicts of interest

There are no conflicts of interest to declare.

## Acknowledgements

This research was supported by JSPS KAKENHI (19H02718) and JST CREST (JPMJCR18R3).

## Notes and references

- 1 H. Liu, L. Zhang, Y. Guo, C. Cheng, L. Yang, L. Jiang, G. Yu, W. Hu, Y. Liu and D. Zhu, *J. Mater. Chem. C*, 2013, **1**, 3104–3109.
- 2 H. Wang, Q. Hao, X. Yang, L. Lu and X. Wang, *Electrochem. Commun.*, 2009, **11**, 1158–1161.
- 3 C. Fu, G. Zhao, H. Zhang and S. Li, *Int. J. Electrochem. Sci.*, 2013, **8**, 6269–6280.
- 4 M. M. Titirici, R. J. White, N. Brun, V. L. Budarin, D. S. Su, F. Del Monte, J. H. Clark and M. J. MacLachlan, *Chem. Soc. Rev.*, 2015, **44**, 250–290.
- 5 Z. Wang and Z. Dai, *Nanoscale*, 2015, **7**, 6420–6431.
- 6 P. Garrigue, M. H. Delville, C. Labrugère, E. Cloutet, P. J. Kulesza, J. P. Morand and A. Kuhn, *Chem. Mater.*, 2004, **16**, 2984–2986.
- 7 W. Choi, I. Lahiri, R. Seelaboyina and Y. S. Kang, *Crit. Rev. Solid State Mater. Sci.*, 2010, **35**, 52–71.
- 8 H. Wang, T. Maiyalagan and X. Wang, *ACS Catal.*, 2012, **2**, 781–794.
- 9 M. Yi and Z. Shen, *J. Mater. Chem. A*, 2015, **3**, 11700–11715.
- 10 X. H. Chen, H. S. Yang, G. T. Wu, M. Wang, F. M. Deng, X. B. Zhang, J. C. Peng and W. Z. Li, *J. Cryst. Growth*, 2000, **218**, 57–61.
- 11 M. Yi and Z. Shen, *Carbon*, 2014, **78**, 622–626.
- 12 A. A. Green and M. C. Hersam, *Nano Lett.*, 2009, **9**, 4031–4036.
- 13 R. Jasti and C. R. Bertozzi, *Chem. Phys. Lett.*, 2010, **494**, 1–7.
- 14 T. H. Vo, M. Shekhirev, D. A. Kunkel, F. Orange, M. J. F. Guinel, A. Enders and A. Sinitskii, *Chem. Commun.*, 2014, **50**, 4172–4174.
- 15 Z. Luo, S. Lim, Z. Tian, J. Shang, L. Lai, B. MacDonald, C. Fu, Z. Shen, T. Yu and J. Lin, *J. Mater. Chem.*, 2011, **21**, 8038–8044.
- 16 T. Morishita, T. Ueno, G. Panomsuwan, J. Hieda, A. Yoshida, M. A. Bratescu and N. Saito, *Sci. Rep.*, 2016, **6**, 1–13.
- 17 T. H. Vo, M. Shekhirev, D. A. Kunkel, M. D. Morton, E. Berglund, L. Kong, P. M. Wilson, P. A. Dowben, A. Enders and A. Sinitskii, *Nat. Commun.*, 2014, **5**, 1–8.
- 18 T. Morishita, T. Ueno, G. Panomsuwan, J. Hieda, A. Yoshida, M. A. Bratescu and N. Saito, *Sci. Rep.*, 2016, **6**, 1–13.
- 19 J. Kang, O. L. Li and N. Saito, *Nanoscale*, 2013, **5**, 6874–6882.
- 20 K. L. Hull, E. L. Lanni and M. S. Sanford, *J. Am. Chem. Soc.*, 2006, **128**, 14047–14049.
- 21 G. Panomsuwan, S. Chiba, Y. Kaneko, N. Saito and T. Ishizaki, *J. Mater. Chem. A*, 2014, **2**, 18677–18686.
- 22 J. Hou, C. Cao, F. Idrees and X. Ma, *ACS Nano*, 2015, **9**, 2556–2564.
- 23 L. Fu, K. Tang, K. Song, P. A. Van Aken, Y. Yu and J. Maier, *Nanoscale*, 2014, **6**, 1384–1389.
- 24 B. Bayatsarmadi, Y. Zheng, C. S. Casari, V. Russo and S. Z. Qiao, *Chem. Commun.*, 2016, **52**, 11947–11950.
- 25 H. Yoon, S. Ko and J. Jang, *Chem. Commun.*, 2007, 1468–1470.
- 26 D. Guo, R. Shibuya, C. Akiba, S. Saji, T. Kondo and J. Nakamura, *Science*, 2016, **351**, 361–365.
- 27 M. M. A. Rafique and J. Iqbal, *Am. J. Phys. Anthropol.*, 2011, **102**, 503–519.